Supplementary Information: Identification of OSSO as a Near-UV Absorber in the Venusian Atmosphere

Benjamin N. Frandsen,[†] Paul O. Wennberg,[‡] and Henrik G. Kjaergaard[*,†]

Department of Chemistry, University of Copenhagen, Universitetsparken 5, 2100 Copenhagen Ø, and Division of Engineering and Applied Science and Division of Geological and Planetary Sciences, California Institute of Technology, Pasadena, California 91125, USA

E-mail: hgk@chem.ku.dk

[*]To whom correspondence should be addressed

[†]Department of Chemistry, University of Copenhagen, Universitetsparken 5, 2100 Copenhagen Ø

[‡]Division of Engineering and Applied Science and Division of Geological and Planetary Sciences, California Institute of Technology, Pasadena, California 91125, USA

Contents

S1 Details on the *Ab Initio* Methods **S3**

S2 *Ab Initio* Calculations of the S_2O_2 Isomers **S4**

S2.1 Geometries of S_2O_2 Isomers and Transition States S4

S2.2 Electronic Transitions S9

S3 Discussion of Other Investigated Molecules **S15**

S3.1 Sulfuric acid analogues S15

S3.2 S_2O S16

S3.3 Radicals: ClSO, $ClSO_2$ and NO_2 . . . . . S17

S4 Rate Constant of OSSO Formation **S18**

S5 Uncertainty in our OSSO Estimate **S24**

S6 Photochemistry of OSSO **S26**

S7 Modeling of SO and review of SO Measurements **S29**

S7.1 Choice of SO_2 Mixing Ratios S31

S1 Details on the *Ab Initio* Methods

The geometries of all the potential near-UV absorbers were initially optimized with density functional theory (DFT) using the functionals: B3LYP, M06-2X and ωB97X-D and using the 6-31+G(d) basis set with default settings. Subsequently, geometries were further optimized with the aug-cc-pV(T+d)Z basis set and the keywords "opt=verytight" and "int=ultrafine".[1–5] Vertical excitation energies (Vee) and oscillator strengths (f) were calculated with time-dependent density functional theory (TD-DFT), using the same functionals and basis sets employed for the optimization and using default settings.

Due to possible partial biradical character of some of the S_2O_2 isomers, the single-reference description might not be sufficient. This problem is well known for S_2O.[6] The multi-reference character of the CCSD(T)/cc-pV(T+d)Z calculations was investigated with the T_1 diagnostic.[7] To further test the multi-reference character, complete active space self-consistent field (CASSCF) calculations on each of the S_2O_2 isomers and transition states were done. The CI-vectors (coefficient >0.05) of the final CASSCF iteration were extracted. The multi-reference character was evaluated for each S_2O_2 isomer and transition state using the [12,12]-CASSCF/aug-cc-pV(T+d)Z method and basis set. The results can be seen in section S2 Table S6, showing that a [2,2]-CAS reference for the MRCI calculations can describe the multi-reference character of the S_2O_2 isomers and transitions states well.

MRCI is not a size extensive method so the energy for ^{3}SO+^{3}SO was calculated with the two ^{3}SO molecules separated by 100 Å to facilitate comparison with S_2O_2 isomers. Calculations on these two separated ^{3}SO molecules with total spin multiplicities of 1 (singlet) and 5 (pentet) were found to have the same energy, indicating that MRCI can treat two non-interacting molecules correctly. The energy difference between two ^{3}SO molecules and trigonal-S_2O_2 were found to be similar with both the CCSD(T) and the MRCI methods. Since ^{3}SO and trigonal-S_2O_2 were found to be well described by CCSD(T), it suggests that our approach to handle the lack of size extensivity in MRCI is reasonable.

S2 *Ab Initio* Calculations of the S_2O_2 Isomers

S2.1 Geometries of S_2O_2 Isomers and Transition States

The MRCI/cc-pV(T+d)Z geometry optimized S_2O_2 isomers and transition states are shown in Figure S1, and the geometric parameters in Table S1 and Table S2.

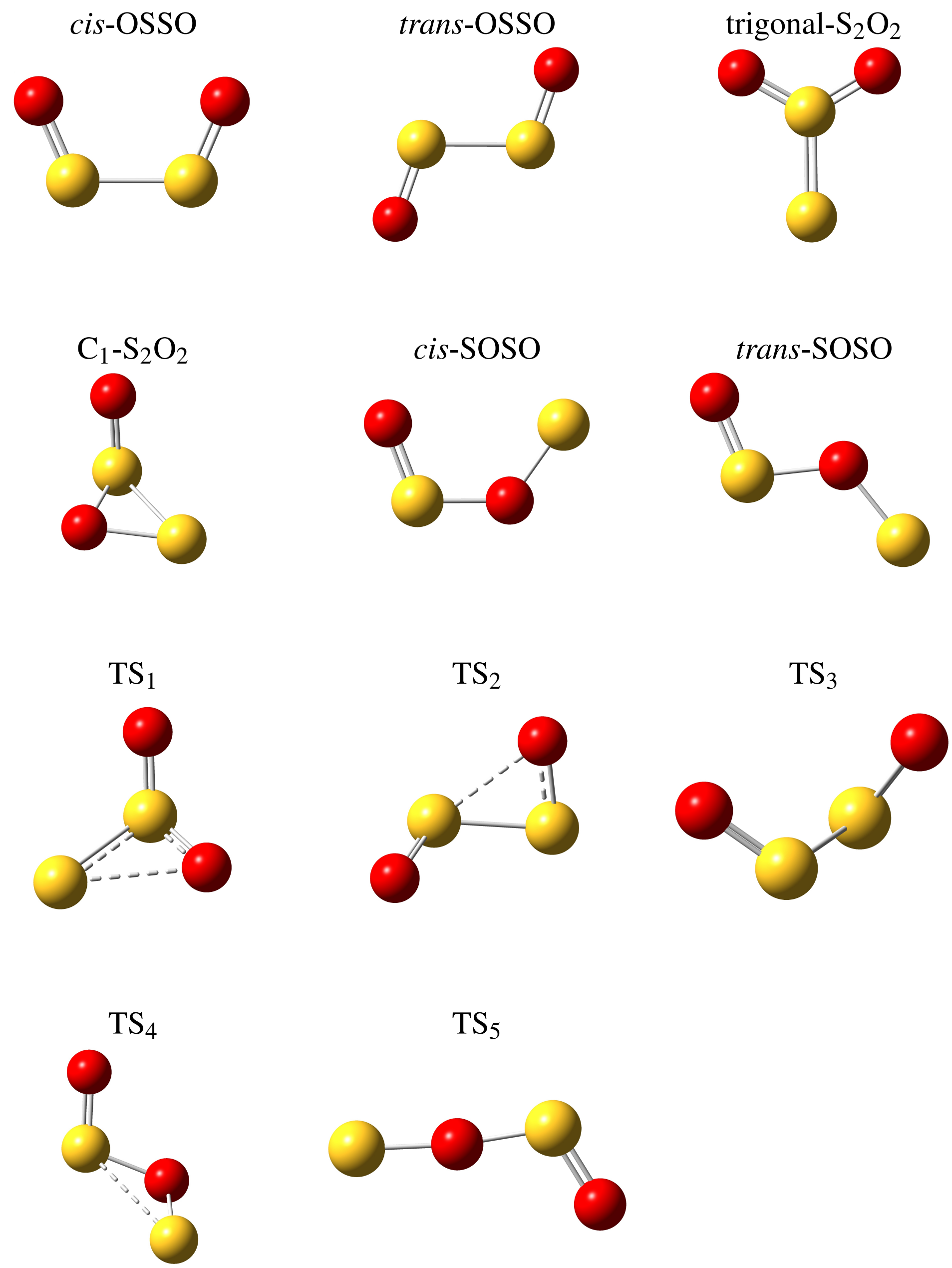

Figure S1: The S_2O_2 isomers and transition states. Dashed lines in the transition states indicate which bonds are broken/formed.

Table S1 and Table S2 lists the MRCI/cc-pV(T+d)Z and CCSD(T)/cc-pV(T+d)Z optimized geometries for the S_2O_2 isomers and transition states and compares with the experimentally determined parameters for *cis*-OSSO.

Table S1: Bond lengths (R) in Å, angles (θ) and dihedral angles (ϕ) in degrees, for the different S_2O_2 isomers and transition states.

	R_{S-S} (Å)	$R_{S=O}$ (Å)	$\theta_{S-S=O}$	$\phi_{O=S-S=O}$
cis-OSSO[a]	1.988	1.449	113.3	0
cis-OSSO[b]	2.0245±0.0006	1.458±0.002	112.7°±0.5	0
trans-OSSO[a]	2.006	1.455	109.1	180
Trigonal-S_2O_2[a]	1.855	1.392	120.3	180

	$R_{O=S}$ (Å)	R_{S-O} (Å)	R_{S-S} (Å)	$\theta_{O=S-O}$	θ_{S-O-S}	$\phi_{O=S-O-S}$
cis-SOSO[a]	1.434	1.610	2.861	110.5	125.9	0
trans-SOSO[a]	1.435	1.630	2.838	106.4	122.3	180
C_1-S_2O_2[a]	1.417	1.776	2.066	112.9	75.4	101.8
TS_1[a]	1.414	1.449	2.104	122.5	58.2	117.8
TS_2[a]	1.434	1.573	1.987	130.8	58.7	89.0
TS_3[a]	1.452	1.452	2.164	102.8	45.0	86.2
TS_4[a]	1.433	1.649	2.621	109.1	106.7	120.4
TS_5[a]	1.429	1.600	3.140	111.7	173.1	180.0

[a]Calculated with MRCI/cc-pV(T+d)Z using a [2,2]-CASSCF reference.

[b]Experimental data from Lovas *et al.*.[8] Note that the calculated bond lengths correspond to an equilibrium geometry, while the experimental bond lengths correspond to zero-point geometries.

Table S2: Bond lengths (R) in Å, angles (θ) and dihedral angles (ϕ) in degrees, for the different S_2O_2 isomers and transition states.[a]

	R_{S-S} (Å)	$R_{S=O}$ (Å)	$\theta_{S-S=O}$	$\phi_{O=S-S=O}$
cis-OSSO	2.026	1.476	113.4	0
trans-OSSO	2.044	1.481	110.1	180
Trigonal-S_2O_2	1.882	1.434	120.2	180

	$R_{O=S}$ (Å)	R_{S-O} (Å)	R_{S-S} (Å)	$\theta_{O=S-O}$	θ_{S-O-S}	$\phi_{O=S-O-S}$
cis-SOSO	1.455	1.614	2.879	111.3	123.4	0
trans-SOSO	1.454	1.665	2.865	108.1	120.6	180
C_1-S_2O_2	1.442	1.780	2.112	115.9	76.4	101.1
TS_1	1.443	1.478	2.085	119.9	58.4	122.2
TS_2	1.459	1.613	2.023	132.4	61.4	91.8
TS_3	1.492	1.492	2.342	104.4	47.6	59.5
TS_4	1.454	1.643	2.666	109.8	106.1	131.3
TS_5	1.449	1.536	3.186	113.7	170.7	179.9

[a]Calculated with CCSD(T)/cc-pV(T+d)Z.

In Table S3, we list the calculated harmonic frequencies - and oscillator strengths for the six S_2O_2 isomers. Optical densities for each vibrational mode in *cis*- and *trans*-OSSO is given in Table S4 using our Model A for OSSO formation. Model A has an SO mixing ratio of 12 ppb and an SO_2 mixing ratio of 120 ppb at 64 km altitude. Model B has a 20 ppb SO mixing ratio and 380 ppb SO_2 mixing ratio at 64 km altitude.

Table S3: Normal mode frequencies (ω) given in wavenumbers (cm^{-1}) and oscillator strength (f) of the S_2O_2 isomers.[a]

	ω_1	f_1	ω_2	f_2	ω_3	f_3
cis-OSSO	162	9.3×10^{-7}	275	0	505	4.9×10^{-6}
trans-OSSO	189	0	209	4.9×10^{-6}	375	0
Trigonal-S_2O_2	379	8.5×10^{-7}	459	0	517	4.4×10^{-6}
C_1-S_2O_2	302	2.0×10^{-7}	462	3.9×10^{-6}	505	7.6×10^{-6}
cis-SOSO	194	8.8×10^{-7}	267	0	538	1.6×10^{-6}
trans-SOSO	75	0	222	5.6×10^{-7}	393	7.6×10^{-7}

	ω_4	f_4	ω_5	f_5	ω_6	f_6
cis-OSSO	526	2.4×10^{-8}	1234	3.0×10^{-5}	1288	1.1×10^{-5}
trans-OSSO	584	0	1231	5.6×10^{-5}	1250	0
Trigonal-S_2O_2	728	7.6×10^{-6}	1313	5.4×10^{-5}	1526	3.8×10^{-5}
C_1-S_2O_2	593	5.7×10^{-6}	894	9.5×10^{-6}	1396	5.6×10^{-5}
cis-SOSO	677	6.9×10^{-6}	971	4.1×10^{-5}	1330	2.5×10^{-5}
trans-SOSO	697	1.5×10^{-5}	977	5.8×10^{-5}	1329	2.9×10^{-5}

[a]Calculated using MRCI/cc-pV(T+d)Z optimized geometries listed in Table S1.

Table S4: Column optical densities (OD) of the vibrational transitions in *cis*- and *trans*-OSSO[a] from our Model A. Model B gives ODs a factor of 2.8 larger than those in Model A.

	OD_1	OD_2	OD_3	OD_4	OD_5	OD_6
cis-OSSO	0.0011	0	0.0057	0.0000	0.0343	0.0126
trans-OSSO	0	0.0010	0	0	0.0113	0

[a]We used a box model 20 cm^{-1} wide for each vibrational transition. Oscillator strengths from Table S3.

In Table S5 the MRCI/cc-pV(T+d)Z and CCSD(T)/cc-pV(T+d)Z ZPVE corrected electronic energies are listed for the geometry optimized S_2O_2 isomers and transition states relative to $^3SO+^3SO$. In Table S6 the CI-vectors and T_1 diagnostic values are listed for each S_2O_2 isomer and transition state. We find that all S_2O_2 isomers and transition states are described qualitatively correct by a

[2,2]-CAS wavefunction.

Table S5: The zero-point vibrational energy corrected electronic energies (E+ZPVE in kJ/mol) for the S_2O_2 isomers and transitions states relative to two free ^{3}SO molecules.

	CCSD(T)	MRCI
cis-OSSO	-107.5	-90.8
trans-OSSO	-98.7	-84.6
Trigonal-S_2O_2	-155.8	-152.6
C_1-S_2O_2	-81.6	-72.6
cis-SOSO	-27.6	-23.6
trans-SOSO	-3.3	-5.6
TS_1	44.4	78.9
TS_2	12.0	44.5
TS_3	32.8	-1.4
TS_4	0.2	7.0
TS_5	33.9	36.0
^{3}SO+^{3}SO	0	0

Table S6: The T_1 diagnostic from CCSD(T)/cc-pV(T+d)Z geometry optimization, and the norm of the two largest CI vectors, (in %) from [12,12]-CASSCF/aug-cc-pV(T+d)Z geometry optimization of the S_2O_2 isomers and transition states.

	T_1 diagnostic	First CI vector	Second CI vector
cis-OSSO	0.024	88.5	3.0
trans-OSSO	0.025	87.9	3.9
Trigonal-S_2O_2	0.019	90.6	0.8
C_1-S_2O_2	0.023	90.0	1.3
cis-SOSO	0.038	70.9	22.0
trans-SOSO	0.047	64.9	28.1
TS_1	0.032	76.3	13.3
TS_2	0.048	87.7	3.0
TS_3	0.028	46.3	45.3
TS_4	0.067	72.7	19.0
TS_5	0.033	46.5	45.0

S2.2 Electronic Transitions

We have calculated the vertical excitation energy (Vee) and oscillator strength (f) of the first six electronic transitions of each symmetry for the S_2O_2 isomers. We used the CC2/aug-cc-pV(T+d)Z method on the MRCI/cc-pV(T+d)Z optimized geometries and each of the results are listed in Table S7, Table S8, Table S9, Table S10, Table S11 and Table S12.

Table S7: Calculated vertical excitation energies (Vee) and oscillator strengths (f) in *cis*-OSSO.[a]

Assignment	Vee (eV)	Vee (nm)	f
$1A_2$	2.80	443	0[b]
$1B_2$	3.97	313	0.08891
$1B_1$	4.01	310	0.00017
$2A_1$	4.06	305	0.00331
$2B_1$	5.02	247	0.00049
$2A_2$	6.01	206	0[b]
$2B_2$	6.17	201	0.00088
$3B_2$	6.64	187	0.32294
$3B_1$	6.76	183	0.00088
$3A_1$	6.81	182	0.05932
$4A_1$	6.93	179	0.07708
$4B_1$	6.94	179	0.04499
$5B_1$	7.61	163	0.02302
$3A_2$	7.62	163	0[b]
$4B_2$	7.63	163	0.02468
$5A_1$	7.66	162	0.02259
$6A_1$	7.83	158	0.07494
$4A_2$	7.87	158	0[b]
$6B_1$	7.90	157	0.00149
$5A_2$	7.98	155	0[b]
$5B_2$	8.16	152	0.09721
$7A_1$	8.20	151	0.00509
$6B_2$	8.30	150	0.06960
$6A_2$	8.41	148	0[b]

[a]Calculated with CC2/aug-cc-pV(T+d)Z on the MRCI/cc-pV(T+d)Z optimized geometry. *Cis*-OSSO has C_{2v} symmetry and the ground state is A_1 symmetry.

[b]Electronic transitions to an A_2 state are forbidden by symmetry.

Table S8: Calculated vertical excitation energies (Vee) and oscillator strengths (f) in *trans*-OSSO.[a]

Assignment	Vee (eV)	Vee (nm)	f
$1B_g$	2.48	501	0[b]
$1B_u$	3.35	370	0.09392
$2B_g$	4.11	302	0[b]
$2B_u$	4.36	284	0.01975
$1A_u$	4.79	259	0.00035
$3B_g$	5.74	216	0[b]
$2A_g$	6.24	199	0[b]
$4B_g$	6.45	192	0[b]
$2A_u$	6.45	192	0.01736
$3B_u$	6.53	190	0.29376
$3A_g$	6.54	190	0[b]
$4A_g$	6.74	184	0[b]
$3A_u$	7.41	167	0.00627
$5A_g$	7.49	166	0[b]
$4A_u$	7.51	165	0.00011
$5B_g$	7.56	164	0[b]
$5A_u$	7.66	162	0.01882
$4B_u$	7.67	162	0.16101
$6A_g$	7.74	160	0[b]
$5B_u$	8.00	155	0.00717
$6A_u$	8.01	155	0.00381
$7A_g$	8.10	153	0[b]
$6B_g$	8.27	150	0[b]
$6B_u$	8.41	147	0.04564

[a]Calculated with CC2/aug-cc-pV(T+d)Z on the MRCI/cc-pV(T+d)Z optimized geometry. *Trans*-OSSO has C_{2h} symmetry and the ground state is A_g symmetry.

[b]Electronic transitions to the A_g and B_g states are forbidden by symmetry

Table S9: Calculated vertical excitation energies (Vee) and oscillator strengths (f) in trigonal-S_2O_2.[a]

Assignment	Vee (eV)	Vee (nm)	f
$1A_2$	3.96	313	0^b
$1B_2$	4.55	273	0.00134
$1B_1$	5.38	231	0.00492
$2A_1$	5.74	216	0.11743
$2A_2$	6.60	188	0^b
$2B_1$	6.88	180	0.00063
$2B_2$	7.07	176	0.00117
$3A_2$	7.24	171	0^b
$3B_2$	7.31	170	0.00852
$3A_1$	7.68	162	0.09866
$4B_2$	7.78	159	0.10584
$5B_2$	8.25	150	0.07591
$3B_1$	8.37	148	0.03849
$4A_2$	8.50	146	0^b
$4A_1$	8.61	144	0.33564
$5A_1$	9.01	138	0.18359
$6B_2$	9.15	136	0.00062
$5A_2$	9.18	135	0^b
$4B_1$	9.27	134	0.04572
$6A_1$	9.59	129	0.00047
$6A_2$	9.60	129	0^b
$5B_1$	10.23	121	0.01082
$6B_1$	10.28	121	0.00206
$7A_1$	10.32	120	0.01933

[a]Calculated with CC2/aug-cc-pV(T+d)Z on the MRCI/cc-pV(T+d)Z optimized geometry. Trigonal-S_2O_2 has C_{2v} symmetry and the ground state is A_1 symmetry.

[b]Electronic transitions to an A_2 state are forbidden by symmetry.

Table S10: Calculated vertical excitation energies (Vee) and oscillator strengths (f) in C_1-S_2O_2.[a]

Assignment	Vee (eV)	Vee (nm)	f
2A	3.12	397	0.00420
3A	4.07	305	0.01993
4A	4.73	263	0.22634
5A	5.35	232	0.45592
6A	5.57	223	0.12653
7A	6.35	195	0.05439

[a]Calculated with CC2/aug-cc-pV(T+d)Z on the MRCI/cc-pV(T+d)Z optimized geometry.

Table S11: Vertical excitation energies (Vee) and oscillator strengths (f) in *cis*-SOSO.[a]

Assignment	Vee (eV)	Vee (nm)	f
1A”	1.28	971	0.00001
2A’	3.31	375	0.07847
3A’	3.67	338	0.11878
2A”	4.33	287	0.00002
4A’	4.63	268	0.01534
3A”	4.71	264	0.00145
4A”	5.45	228	0.00196
5A’	5.52	225	0.09374
6A’	5.92	210	0.00005
5A”	6.27	198	0.00006
6A”	6.40	194	0.00019
7A’	6.55	189	0.02011

[a]Calculated with CC2/aug-cc-pV(T+d)Z on the MRCI/cc-pV(T+d)Z optimized geometry. *Cis*-SOSO has C_s symmetry and the ground state is A’ symmetry.

Table S12: Vertical excitation energies (Vee) and oscillator strengths (f) in *trans*-SOSO.[a]

Assignment	Vee (eV)	Vee (nm)	f
1A”	1.06	1169	0.00017
2A’	2.76	449	0.11605
3A’	3.73	332	0.04810
2A”	4.15	299	0.00004
4A’	4.39	282	0.01370
3A”	4.53	274	0.00032
4A”	5.08	244	0.00154
5A’	5.57	223	0.09848
6A’	5.91	210	0.04657
5A”	5.95	209	0.00067
7A’	6.05	205	0.00729
6A”	6.10	203	0.00320

[a]Calculated with CC2/aug-cc-pV(T+d)Z on the MRCI/cc-pV(T+d)Z optimized geometry. *Trans*-SOSO has C_s symmetry and the ground state is A’ symmetry.

To ensure that the electronic transition energies and oscillator strengths were converged, we employed a progression of improved methods from CC2 to CC3 and basis set from double zeta to quadruple zeta quality. We list the energy and oscillator strength of the dominant electronic transition in the 300-400 nm wavelength region of *cis*- and *trans*-OSSO in Table S13 and Table S14. It is clear that only minor changes occur in the transition energy and oscillator strength as we change method and basis set.

The effect of including the zero-point vibrational energy correction, from the vibration along the S-S bond, to the vertical excitation energies is a red-shift of less than 4 nm for the 364 nm transition in *trans*-OSSO and less than 3 nm for the 316 nm transition in *cis*-OSSO.

Table S13: Calculated vertical excitation energy (Vee) and oscillator strength (f) in *cis*-OSSO from the $1A_1$ state to the $1B_2$ state.[a]

Vee (nm)	CC2	CCSD	CC3
aug-cc-pV(D+d)Z	310	310	313
aug-cc-pV(T+d)Z	313	313	316
aug-cc-pV(Q+d)Z	313	313	-[b]

Oscillator strength	CC2	CCSD	CC3
aug-cc-pV(D+d)Z	0.08751	0.08972	0.07665
aug-cc-pV(T+d)Z	0.08891	0.09199	0.07716
aug-cc-pV(Q+d)Z	0.08850	0.09249	-[b]

[a]Calculated with linear response coupled cluster calculations (LR-CC) on the MRCI/cc-pV(T+d)Z optimized geometry.

[b]Calculation could not be done due to time and computer memory constraints.

Table S14: Calculated vertical excitation energy (Vee) and oscillator strength (f) in *trans*-OSSO from the $1A_g$ state to the $1B_u$ state.[a]

Vee (nm)	CC2	CCSD	CC3
aug-cc-pV(D+d)Z	367	359	359
aug-cc-pV(T+d)Z	370	363	364
aug-cc-pV(Q+d)Z	370	363	-[b]

Oscillator strength	CC2	CCSD	CC3
aug-cc-pV(D+d)Z	0.09583	0.09031	0.07505
aug-cc-pV(T+d)Z	0.09391	0.08954	0.07357
aug-cc-pV(Q+d)Z	0.09312	0.08949	-[b]

[a]Calculated with linear response coupled cluster calculations (LR-CC) on the MRCI/cc-pV(T+d)Z optimized geometry.

[b]Calculation could not be done due to time and computer memory constraints.

S3 Discussion of Other Investigated Molecules

S3.1 Sulfuric acid analogues

The rapid sulfuric acid production on Venus in the upper cloud layer, suggests sulfuric acid analogues could be produced in large quantities. We optimized the geometry and investigated the electronic transitions of sulfurous acid (H_2SO_3), thiosulfuric O-acid (H_2SO_3S), thiosulfuric S-acid (HSO_3SH) and chlorosulfonic acid (HSO_3Cl). The lowest energy electronic transition of each is listed in Table S15. Sulfuric acid was included for reference and the present results are in excellent agreement with previous calculations.[9] The lowest lying vertical excitation energy and oscillator strength of these molecules are all very far from the 320-400 nm wavelength range, indicating that they cannot be the unknown near-UV absorber(s).

Table S15: Vertical excitation energy (Vee) and oscillator strength (f) of sulfuric acid and its analogue molecules.

Molecule	Vee (nm)	f
Sulfurous acid (H_2SO_3)[a]	176	0.0501
Thiosulfuric O-acid (H_2SO_3S)[a]	201	0.0082
Thiosulfuric S-acid (HSO_3SH)[a]	235	0.0017
Chlorosulfonic acid (HSO_3Cl)[a]	196	0.0055
Sulfuric acid (H_2SO_4)[a]	156	0.0077
Sulfuric acid[b]	154	0.0058

[a]Calculated with CC2/aug-cc-pV(T+d)Z on the CCSD(T)/cc-pV(T+d)Z optimized geometries.

[b]Vertical excitation energy calculated with CC3/aug-cc-pV(D+d)Z+3. Oscillator strength calculated with CC3/aug-cc-pV(D+d)Z.[9]

S3.2 S_2O

In Table S16 we list the calculated first 6 electronic transitions in S_2O. It is seen that the oscillator strength of the 446 nm and 388 nm transitions is less than 10^{-4} which is more than 3 orders of magnitude smaller than for *cis*-OSSO or *trans*-OSSO. In addition, previous models do not produce enough S_2O to explain the unexplained near-UV absorption and our present calculations corroborate this.[10,11] The 261 nm absorption is relatively strong but far from the 320-400 nm wavelength range, but could interfere with SO_2 measurements at wavelengths around 261 nm.

Table S16: Calculated vertical excitation energies (Vee) and oscillator strengths (f) in S_2O.[a]

Assignment	Vee (nm)	f
1A”	446	0.00004
2A”	388	0.00007
2A’	261	0.07769
3A’	189	0.00421
4A’	180	0.00080
3A”	170	0.00104

[a]Calculated with CC2/aug-cc-pV(T+d)Z on the MRCI/cc-pV(T+d)Z optimized geometry. S_2O has C_s symmetry and the ground state is A’.

S3.3 Radicals: ClSO, $ClSO_2$ and NO_2

NO_2 is a well known absorber in the 300-500 nm range,[12] and according to our ωB97X-D/6-311+G(2d) geometry optimization and TD-DFT calculations, ClSO, $ClSO_2$ and NO_2 can all absorb in the 320-400 nm wavelength range. The model in Zhang *et al*.[13] predict a mixing ratio for ClSO and $ClSO_2$ around 0.5 ppb and less than 0.01 ppb of NO_2 at 64 km altitude, our model predict *cis*- and *trans*-OSSO mixing ratios larger 2 ppb around 64 km altitude. In Table S17 we compare the dominant electronic transition for the three radicals with those in *cis*- and *trans*-OSSO. It clearly shows that ClSO, $ClSO_2$ and NO_2 are insignificant as near-UV absorbers on Venus in comparison to OSSO.

Table S17: Calculated vertical excitation energy (Vee) and oscillator strength (f) in ClSO, $ClSO_2$, NO_2, *cis*-OSSO and *trans*-OSSO.[a]

	Vee (nm)	f
ClSO	384	0.0006
$ClSO_2$	353	0.0159
NO_2	375	0.0092
cis-OSSO	350	0.0864
trans-OSSO	398	0.0867

[a]Calculated with ωB97X-D/6-311+G(2d).

S4 Rate Constant of OSSO Formation

A simplified scheme of the chemical pathways for the sulfur oxides in the Venusian atmosphere is shown in Figure S2. To assess whether *cis*-OSSO, *trans*-OSSO, *cis*-SOSO and *trans*-SOSO formation is barrierless or not, we scanned the central S-S bond in each OSSO isomer. We illustrate the 3-D potential energy surface in Figure S3.

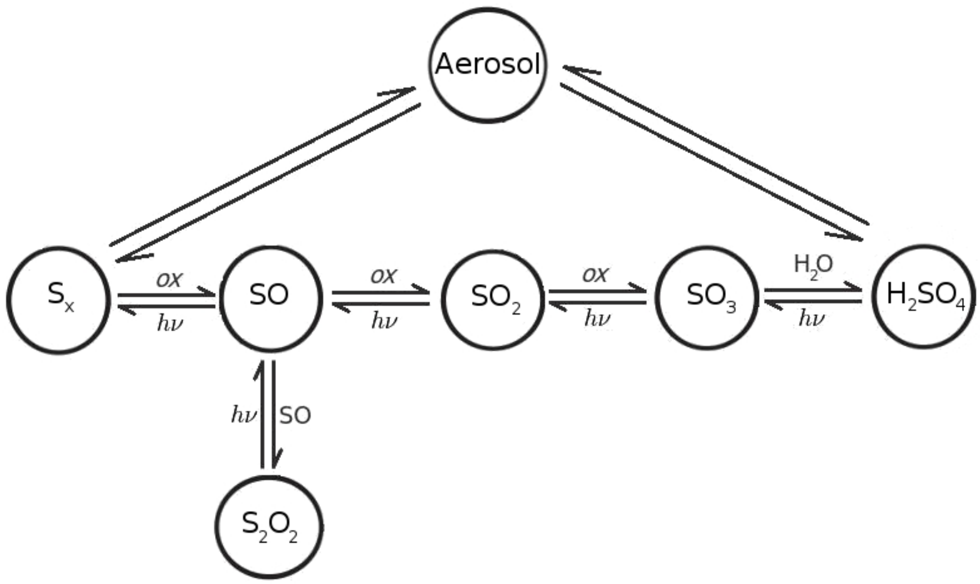

Figure S2: The chemical pathways for the most abundant sulfur oxides in the Venusian atmosphere.

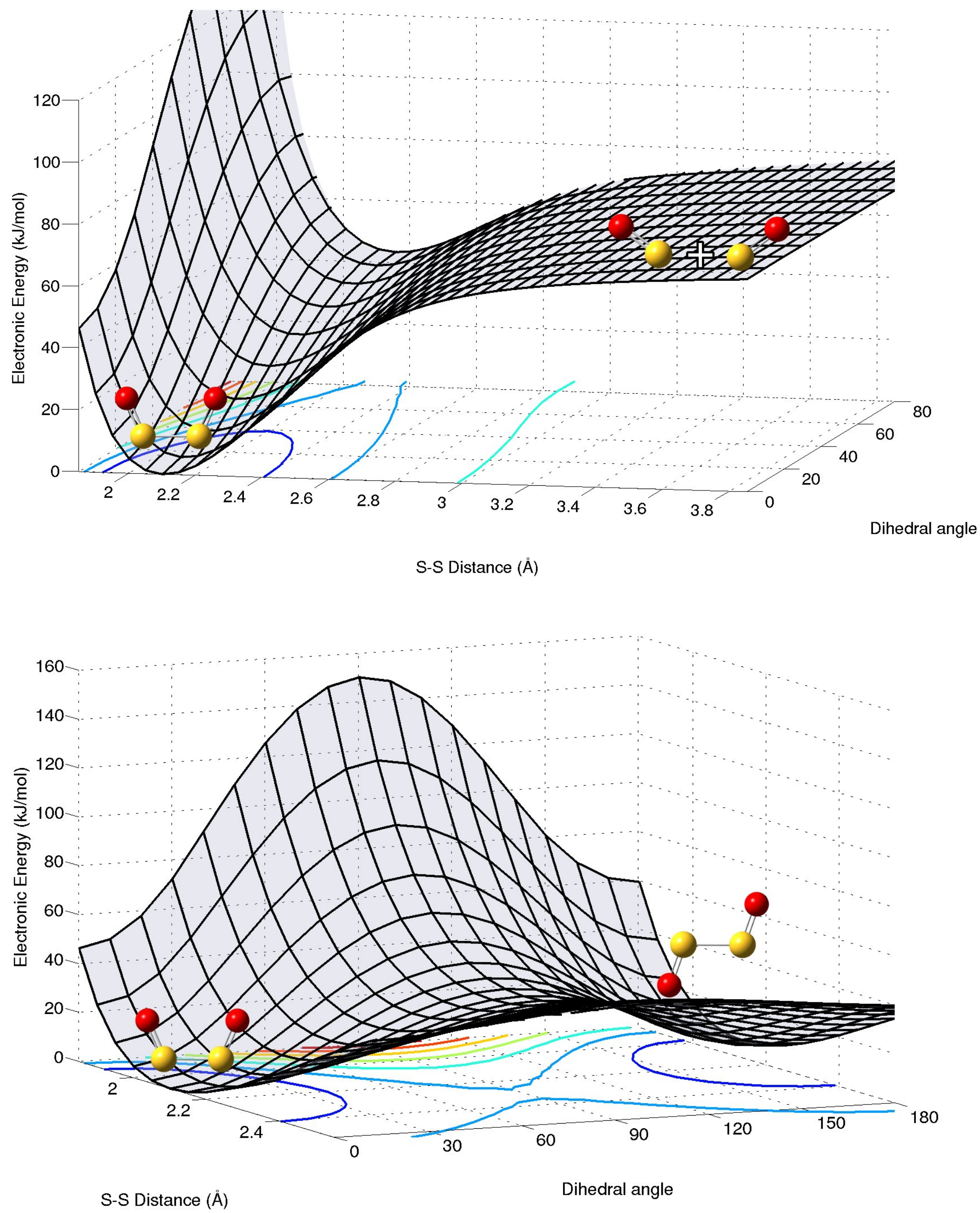

Figure S3: Potential energy surface of *cis*- and *trans*-OSSO formation using the unrestricted B3LYP/6-31G+(d) method with the keywords guess=(mix,always) and with symmetry turned off. The two scan variables was the distance (in Å) between the two S atoms and the O-S-S-O dihedral angle. Internal coordinates other than the scan variables were frozen. Top figure illustrate the barrierless formation of *cis*-OSSO. Bottom figure shows the transition state TS_3 between *cis*- and *trans*-OSSO. Contour lines at the bottom of each figure are in 20 kJ/mol increments, going from blue (dark blue at 20 kJ/mol) to higher energies in red.

The search for a barrier was also performed at the RI-SCS-MP2/cc-pVDZ level of theory, where we scanned the S-S distance from 1.85 Å to 6.00 Å in 80 equidistant steps in the two OSSO isomers, and from 1.40 Å to 6.00 Å in 90 equidistant steps for the two SOSO isomers. The method was set to search for a transition state along the potential energy surface (keyword "ScanTS"), however in all four cases no transition state was found. We conclude that the formation of the two OSSO and the two SOSO isomers is barrierless. The full mechanism of OSSO formation takes the form:

$$^{3}\mathrm{SO} + {}^{3}\mathrm{SO} \underset{k_{-1}}{\overset{k_1}{\rightleftharpoons}} \mathrm{OSSO}^{*} \tag{1}$$

$$\mathrm{OSSO}^{*} + \mathrm{M} \xrightarrow{k_2} \mathrm{OSSO} + \mathrm{M}^{*} \tag{2}$$

The intermediate $OSSO^*$ is 1/9 times singlet, 3/9 times triplet and 5/9 times quintet, which is a consequence of the resulting electronic degeneracy of each possible intermediate state.[14] Singlet OSSO is simply *cis*- and *trans*-OSSO, which is presumably formed in equal amounts upon collision, due to the 86.2° dihedral angle in TS_3 (see Table S1). The triplet potential energy surface has a minimum that resembles the transition state between *cis*- and *trans*-OSSO, TS_3, and earlier DFT studies on the S_2O_2 isomers have successfully identified ^{3}OSSO, and found it to be ∼55 kJ/mol lower in energy than ^{3}SO+^{3}SO, while still being ∼70 kJ/mol higher in energy than cis-OSSO.[15,16] With the CCSD(T)/cc-pV(T+d)Z calculations, we found ^{3}OSSO to be 32 kJ/mol lower in energy than ^{3}SO+^{3}SO. The potential energy surface stationary point corresponding to ^{3}OSSO intersects with the singlet OSSO potential energy surface around TS_3. This enables triplet conversion to singlet, which is limited by spin-orbit coupling in ^{3}OSSO. ^{5}OSSO has no minimum on the potential energy surface since the electrons that are supposed to form a bond between the sulfur atoms have parallel spins. We tested this assumption with DFT and found no minimum on the potential energy surface for ^{5}OSSO. Any ^{5}OSSO intermediate formed upon ^{3}SO + ^{3}SO collision will fall apart rapidly.

In the high pressure limit, singlet and triplet $OSSO^*$ will have a $k_2[M] >> k_{-1}$ and we assume that ^{3}OSSO becomes ^{1}OSSO *via* intersystem crossing. We find that 4 in 9 collisions between SO will have a favourable spin that results in singlet *cis*- or *trans*-OSSO formation. We assume 1/4 of all ^{3}SO+^{3}SO collisions have favourable geometries, since there is roughly 1/4 chance that the sulfur atom of each ^{3}SO molecule will be the colliding part. Thus 1 in 9 of all ^{3}SO+^{3}SO collisions will form *cis* or *trans*-OSSO according to our estimate. We estimate a rate constant with simple collision theory, k_t, for *cis* and *trans*-OSSO formation:

$$\frac{d[\mathrm{OSSO}]}{dt} = k_\mathrm{t}\,[^3\mathrm{SO}]^2 \tag{3}$$

$$k_\mathrm{t} = \left(\frac{8\pi k_\mathrm{B}\mathrm{T}}{\mu}\right)^{\frac{1}{2}} \mathrm{d}^2\mathrm{P}_\mathrm{react} \tag{4}$$

where $\mathrm{P}_\mathrm{react}$ denotes the fraction of collisions that leads to product formation, which we estimated was 1/9. μ denotes the reduced mass of the two molecules involved in the reaction. We assume d = 3 Å based on the B3LYP/6-31+G(d) and the RI-SCS-MP2 potential energy surface scans. In the 64-75 km altitude region on Venus, the temperature is around T=245 K. In this region the resulting k_t is $1.4\times10^{-11}\mathrm{cm}^3\mathrm{s}^{-1}$. For comparison, the two-body limit rate constant given in Zhang *et al.* is k_Zhang=$1.00\times10^{-11}\mathrm{cm}^3\mathrm{s}^{-1}$.[13] This rate constant is estimated as 0.1 times the 2S+M→S_2+M rate constant. We use our calculated k_t as k_∞ in our model for OSSO formation. We assume that k_∞ has a temperature dependence of $\mathrm{T}^{-0.5}$ which is consistent with collision theory. To give a good estimated rate constant for different altitudes we use the Troe scheme to modify the "in-between" high and low pressure limited rate constants.[17] The Troe rate constant is given *via* the formula:

$$k_\mathrm{Troe} = \frac{k_0[\mathrm{M}]}{1+k_0[\mathrm{M}]/k_\infty} F_c^{\left(1+\left(\log_{10}(k_0[\mathrm{M}]/k_\infty)\right)^2\right)^{-1}}, \tag{5}$$

where [M] is the atmospheric number density and F_c is a fitted parameter here taken as 0.6. We have assumed that the temperature dependence of k_0 is (300 K/T)$^{2.4}$, which is chosen to be similar to the temperature dependence of other comparable atmospheric reactions.[13,18] The resulting altitude dependent Troe rate constant is given in Figure S4.

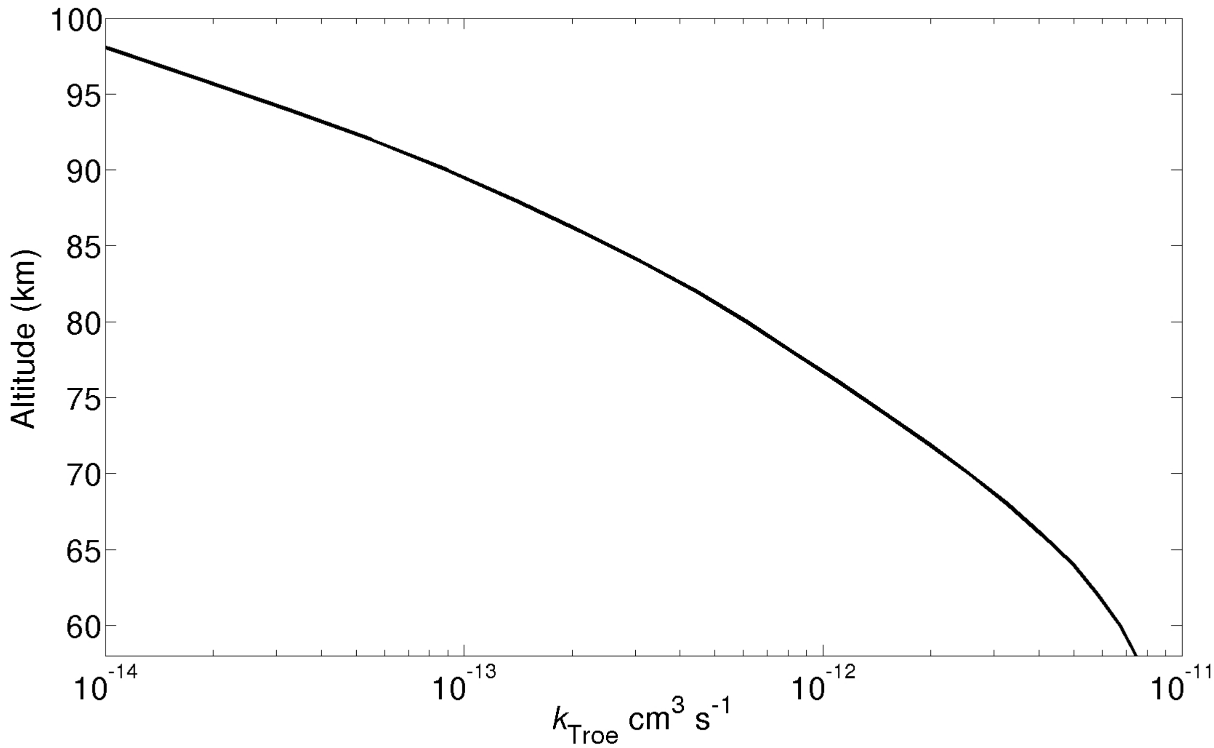

Figure S4: The altitude dependent formation rate of OSSO given by the Troe scheme. Raw data are available in electronic form.

Collisions between the sulfur atom in one ^{3}SO and the oxygen atom in another can produce *cis*- or *trans*-SOSO, which through intramolecular reactions can lead to C_1-S_2O_2 formation. We solved the master equation for the system seen in the main manuscript as Figure 1, however excluding TS_1, TS_2 and TS_3 due to their high energy. Photolysis rate constants for *cis*-OSSO and *trans*-OSSO were are those given in Figure S5 at 64 km altitude. For C_1-S_2O_2 we used the oscillator strength of both the first and second electronic transition given in Table S10 and simulated the absorption cross section using a box model 0.6 eV wide for each transition. We assumed the formation rate constant of *cis*- and *trans*-SOSO from ^{3}SO+^{3}SO collision was 1/4th of that of *cis*- and *trans*-OSSO since there seems to be no stable intermediate triplet state of the SOSO species.

We used the relative energies given in Table S5 to calculate the unimolecular rate constants with the thermodynamic formulation of transition state theory

$$k = \frac{k_{\mathrm{B}}\mathrm{T}}{h}\frac{\mathrm{Q}^{\mathrm{TS}}}{\mathrm{Q}_r} exp\left(\frac{-(\mathrm{E}_{\mathrm{TS}} - \mathrm{E}_r)}{\mathrm{RT}}\right) \quad (6)$$

where the temperature, T, is set to 245 K. Q^{TS} and Q_r are the transition state and reactant partition functions, which we ignored in our estimate as we assume them to be similar. The relative energy between transition state and reactant is $E_{TS}-E_r$. We set the mixing ratio of SO to a constant 12 ppb and used an atmospheric number density of $3.4\times10^{18}\mathrm{cm}^{-3}$. The resulting yields for each of the involved S_2O_2 isomers are listed in Table S18.

Table S18: Yield in percent for the S_2O_2 isomers by solving the master equation for a system involving these and sulfur monoxide. Calculations carried out using dayside conditions on Venus at 64 km altitude.

	Yield in %
cis-OSSO	69.3
trans-OSSO	28.9
C_1-S_2O_2	1.8
cis-SOSO	0.0
trans-SOSO	0.0

S5 Uncertainty in our OSSO Estimate

The rate of OSSO formation is dependent on the square of the SO number density. This makes our estimate of the abundance of OSSO highly sensitive to the assumed SO number density. Thus, uncertainty in the observations of the SO mixing ratio on Venus gives rise to the greatest uncertainty in our OSSO formation estimate. Natural variations in SO concentration on Venus will also affect the OSSO formation rate.

The experimental rate constant for OSSO formation is given at T = 298 K. We assume a $T^{-2.4}$ dependence for the k_0 rate constant consistent with the known temperature dependence of similar association reactions.[13,18] The estimated experimental uncertainty of k_0 is quoted as ±50%. Furthermore, the bath gas (N_2) and pressures used in this experiment (2-8 Torr) were far from Venus conditions in the OSSO formation region (40 to 200 Torr CO_2).[19]

The photolysis quantum yield for OSSO decomposition was assumed $\Phi = 1$, which is an upper limit. In reality the photolysis quantum yield is both smaller and wavelength dependent, but we argue that it is close to 1, which makes the error from this assumption less significant. A lower quantum yield will mean that on average each OSSO absorb more than 1 photon before undergoing photolysis, therefore increasing lifetime and concentration making it a more effective absorber than estimated here.

The calculated electronic transition energies for *cis*- and *trans*-OSSO converges, which means the CC3 computed vertical excitation energies have errors that are insignificant (less than ±3 nm). The oscillator strength from the CC3 calculations are converged to within ±20%, see Table S13, Table S14 and references.[9,20]

In the OSSO photolysis calculation, we chose a Lorentzian line shape with a full width at half maximum of 0.6 eV for the electronic transitions. At 64 km, we obtain a photolysis rate of 0.16 s^{-1} and 0.39 s^{-1} for *cis*- and *trans*-OSSO, respectively. Photolysis is roughly halved for *cis*-OSSO, and ∼30% less for *trans*-OSSO, if we instead use a box model for the absorption cross sections with a width of 0.6 eV. The photolysis rate is less sensitive to line shape and band width above 64 km altitude.

The pressure and temperature profile we used is from Seiff *et al.*[21] which matches latitudes from 0°to 30°, which we consider reliable for this estimate. The actinic flux data are for 45° latitude.[13] We multiplied this actinic flux with $\sqrt{2}$ to match equatorial latitudes.

S6 Photochemistry of OSSO

In Figure S5, we show our calculated altitude dependent photolysis rate constants. Figure S6 shows the Actinic flux at 64, 70 and 80 km altitude on equatorial latitudes on Venus. Note that the actinic flux data are from Zhang *et al.*,[13] which span 58-112 km altitude in 2 km increments and the wavelengths 115.5-800 nm. Here we have scaled their actinic flux values by $\sqrt{2}$ because their data are for the 45° N latitude, while we want equatorial latitudes. The simulated absorption cross section of *cis*- and *trans*-OSSO are shown in Figure S7.

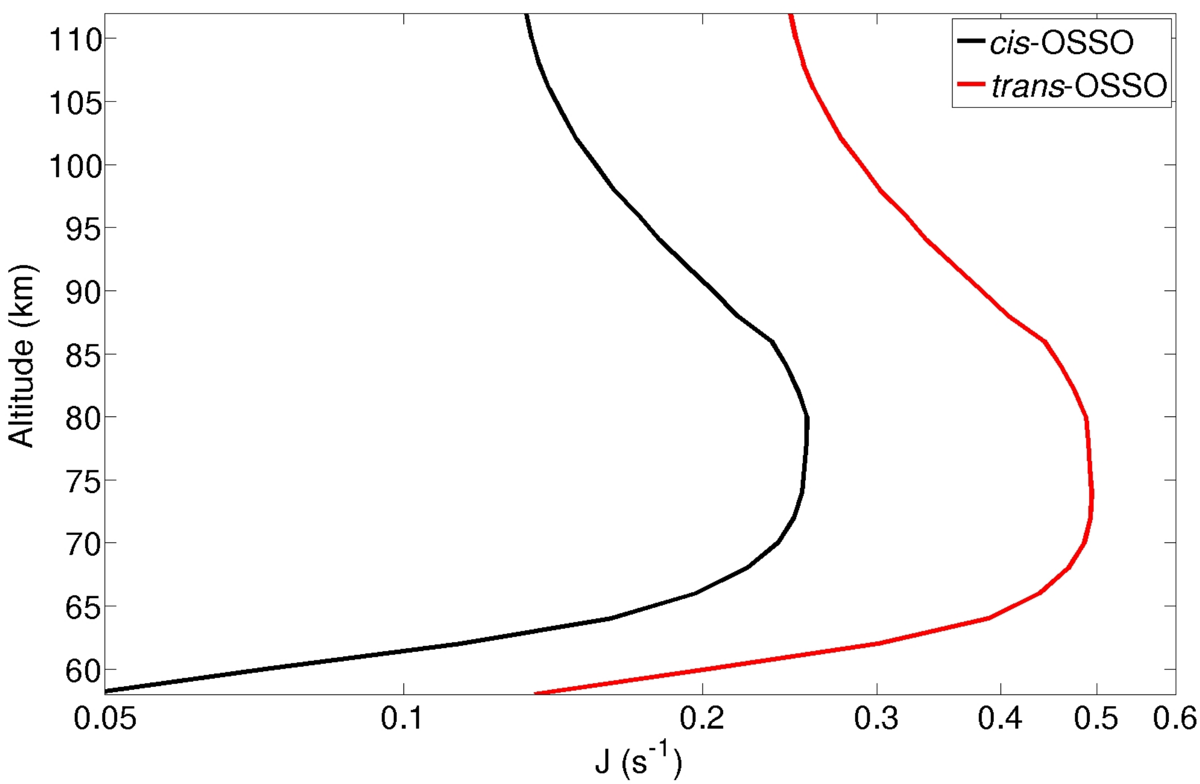

Figure S5: Altitude dependent photolysis rate of *cis*- and *trans*-OSSO assuming a Lorentzian peak shape for the absorption band profile centered at 316 nm and 364 nm for *cis*-OSSO and *trans*-OSSO, respectively, with a FWHM of 0.6 eV.

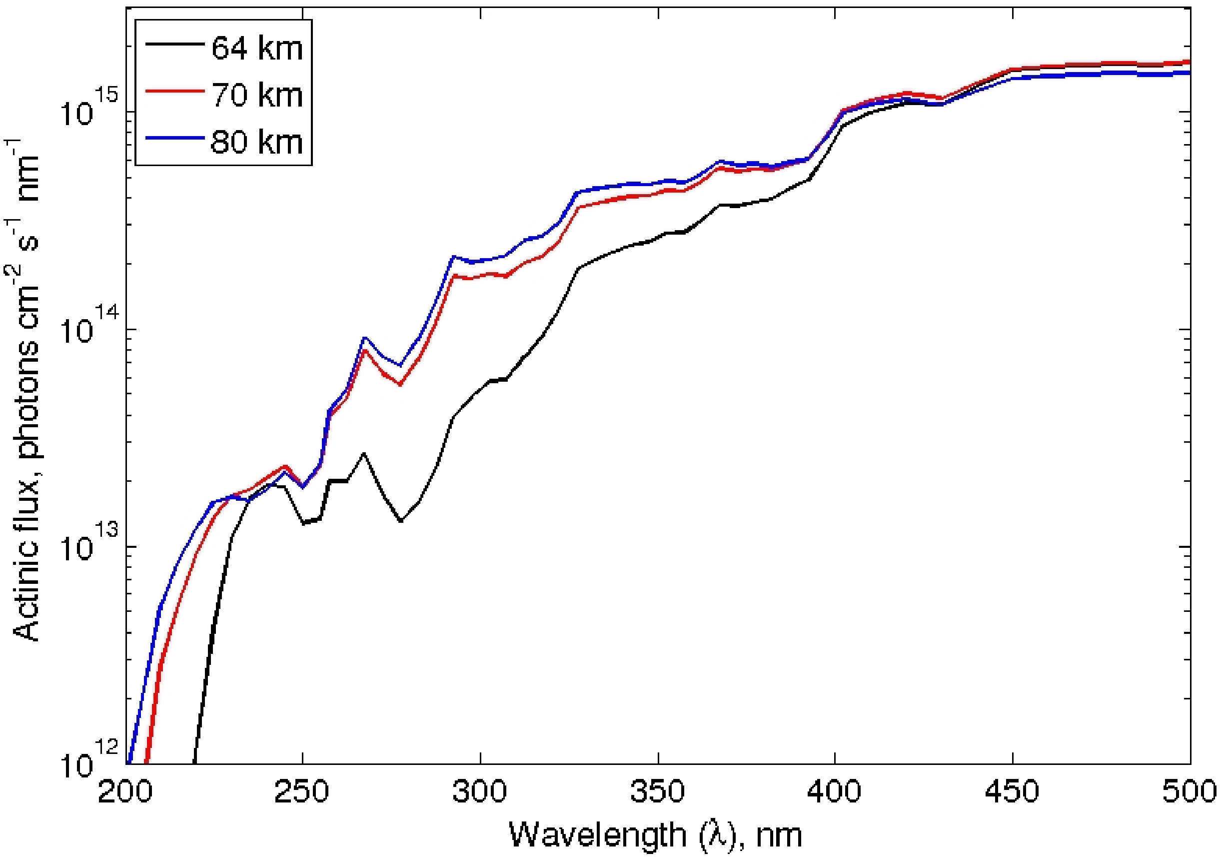

Figure S6: Actinic flux on Venus at equatorial latitudes, at 64, 70 and 80 km altitude. Taken from Zhang *et al.*[13]

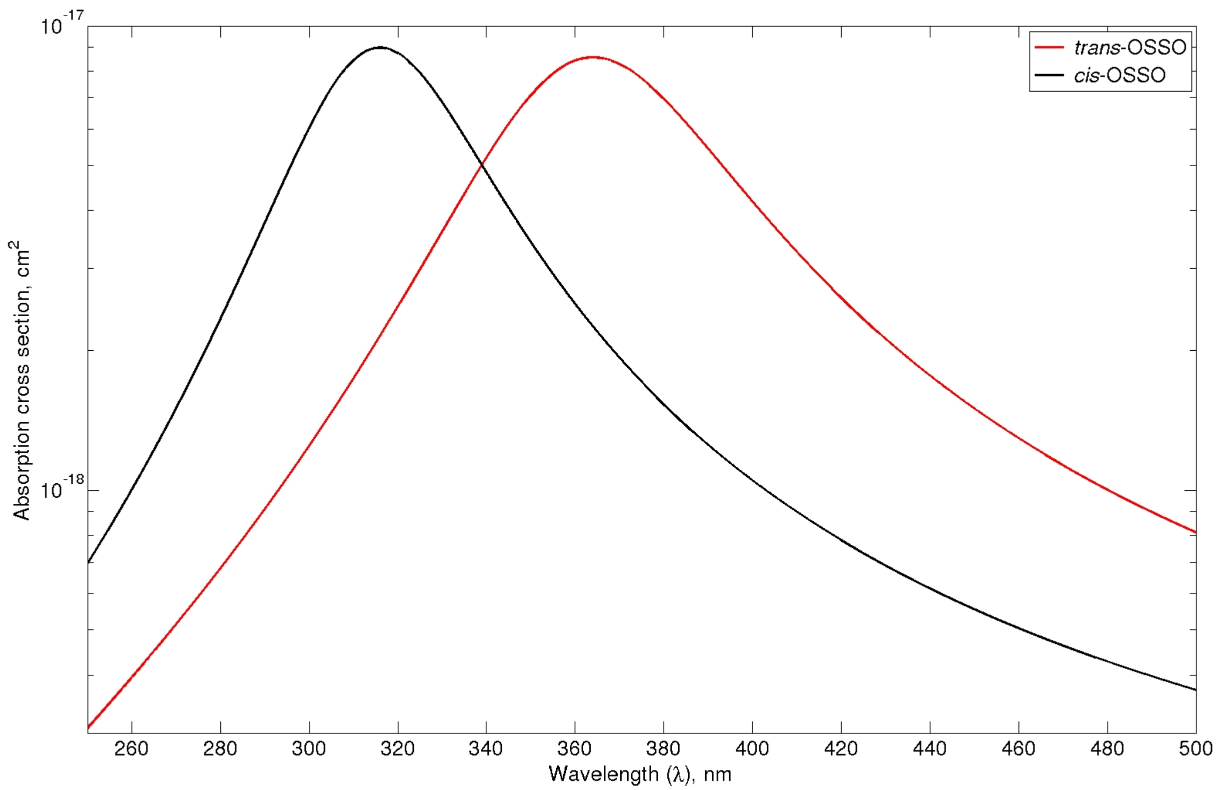

Figure S7: Simulated absorption cross section for *cis*- and *trans*-OSSO using a Lorentzian band shape with full width at half maximum of 0.6 eV. Raw data are available in electronic form.

S7 Modeling of SO and review of SO Measurements

The SO mixing ratio is fixed at altitudes 64 km, 70 km and 96-112 km altitude to 12 ppb (Model A) or 20 ppb (Model B), 3 ppb and 150 ppb, respectively, based on experimental evidence from the literature.[22–25] We model the SO mixing ratio from 58-112 km altitude based on these fix points. From 64 km up to 68 km altitude we let the SO mixing ratio increase slightly due to enhanced SO_2 photolysis at the top of the cloud layer (located at 67±2 km altitude)[26], similarly we let the SO mixing decrease from 64 km down to 58 km altitude due to diminished SO_2 photolysis deeper into the cloud layer. From 70 km and up to 88 km altitude we let the SO mixing ratio moderately increase, consistent with the Sandor *et al*. model C.[23] The SO mixing ratio is then set to increase rapidly until it hits 150 ppb at 96 km altitude. In the 96-112 km altitude regime the SO mixing ratio is kept at a constant of 150 ppb consistent with Belyaev *et al*..[24] See Figure S8 for the altitude dependent SO mixing ratios employed in our two models for OSSO formation on Venus.

The SO mixing ratio of 12 ppb has an uncertainty of ±5 ppb and originate from near-UV sounding rocket experiments in the years 1988-1991.[22] The measurements were done in the 190-230 nm wavelength range, where both SO and SO_2 absorb with similar cross sections.[24] SO_2 concentrations were modeled using the spectral data and SO was included in the model which was shown to give a good fit with 100 ppb SO_2 and 12.5 ppb SO. The Venusian atmosphere was assumed to consist of uniformly mixed CO_2 and sulfuric acid aerosols. The estimated error on SO_2 measurements were 50%, and the calculated scale height of SO_2 was 3±1 km. We refer the reader to the paper by Na *et al.*[22] for all details regarding the measurement of SO concentrations in the atmosphere of Venus. An earlier study from 1987-1988, using a similar model found SO mixing ratios of 20±10 ppb based on measurements in 1979.[25] In Na *et al.* the focus was on SO_2 concentrations and inclusion of SO in their model provided a good fit to spectral data. An improved measurement could include measuring the 240-320 nm range since the SO absorption cross section rapidly declines above 230 nm, while SO_2 continues to absorb in the 230-320 nm wavelength range. Thus we would get a measure of SO_2 concentrations independent of SO, and might be able to better extract SO mixing ratios from measurements in the 190-230 nm range.

The SO mixing ratio of 3 ppb at 70 km altitude are from a model fit to microwave spectra of Venus by Sandor *et al.*.[23] Their "best fit" is a SO mixing ratio of 0 ppb at 70-85 km altitude and 31 ppb at 86-100 km altitude. They point out that both SO and SO_2 have much lower mixing ratios in the 70-85 km altitude regime compared to the 85-100 km altitude regime. We have chosen Sandor *et al.*'s "Model C" of the SO mixing ratio to give a 70 km altitude SO mixing ratio and use their observation of the [SO_2]/[SO] ratio, which has an exponential increase from $\sim$ 77 km altitude to $\sim$ 90 km altitude.

The SO mixing ratio above 90 km altitude is from Belyaev *et al*. who used the Venus Express SPICAV/SOIR measurements.[24] The authors observed an increasing mixing ratio for both SO and SO_2 going from 90 to $\sim$ 96 km altitude. In the 96-104 km altitude range the SO mixing ratio remains constant at around 150 ppb.

The resulting SO and OSSO number densities based the SO mixing ratio shown in Figure S8 Model A, and the described model for OSSO formation with a rate constant plotted in Figure S4 and photolysis rate in Figure S5 are depicted in Figure S9. The Model B SO and OSSO number densities are depicted in Figure S10. While OSSO is enhanced by the increasing SO mixing ratio in the 90-96 km altitude range, its abundance is significant only at altitudes <70 km altitude. A zoomed in version of Figure S9 is in the main manuscript as Figure 2.

S7.1 Choice of SO_2 Mixing Ratios

The inclusion of SO_2 in Figure S9 and Figure S10 is purely illustrative. The two Na *et al.* papers provide both SO and SO_2 mixing ratios.[22,25] Consistent with the SO_2 to SO ratio from the Na *et al.* papers, we adopt their SO_2 mixing ratios and scale heights. For Model A this gives a mixing ratio at at 64 km altitude of 120 ppb and a scale height of 3 km, with uncertainties $\pm$60 ppb and $\pm$1 km. For Model B we get 380 ppb SO_2 at 64 km altitude and a scale height of 3 km, with uncertainties $\pm$70 ppb and $\pm$1 km.

At high altitudes, 85-112 km, we use the same SO_2 profile for both Model A and B. It is the profile from Sandor *et al.*,[23] which simply gives a constant mixing ratio in this range. Therefore, the SO_2 profile follows the scale height of the atmosphere in this range.

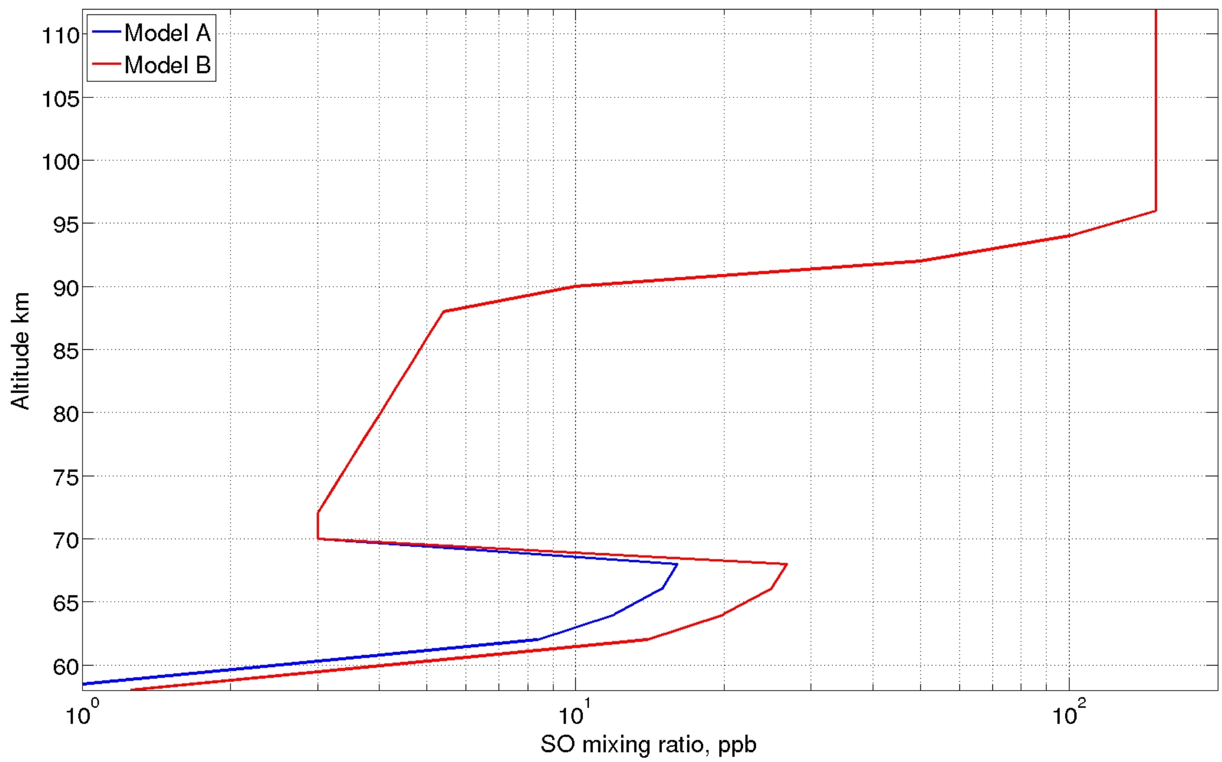

Figure S8: The altitude dependent SO mixing ratio used in our two models for OSSO formation. Model A and B are identical from 70 km altitude and above.

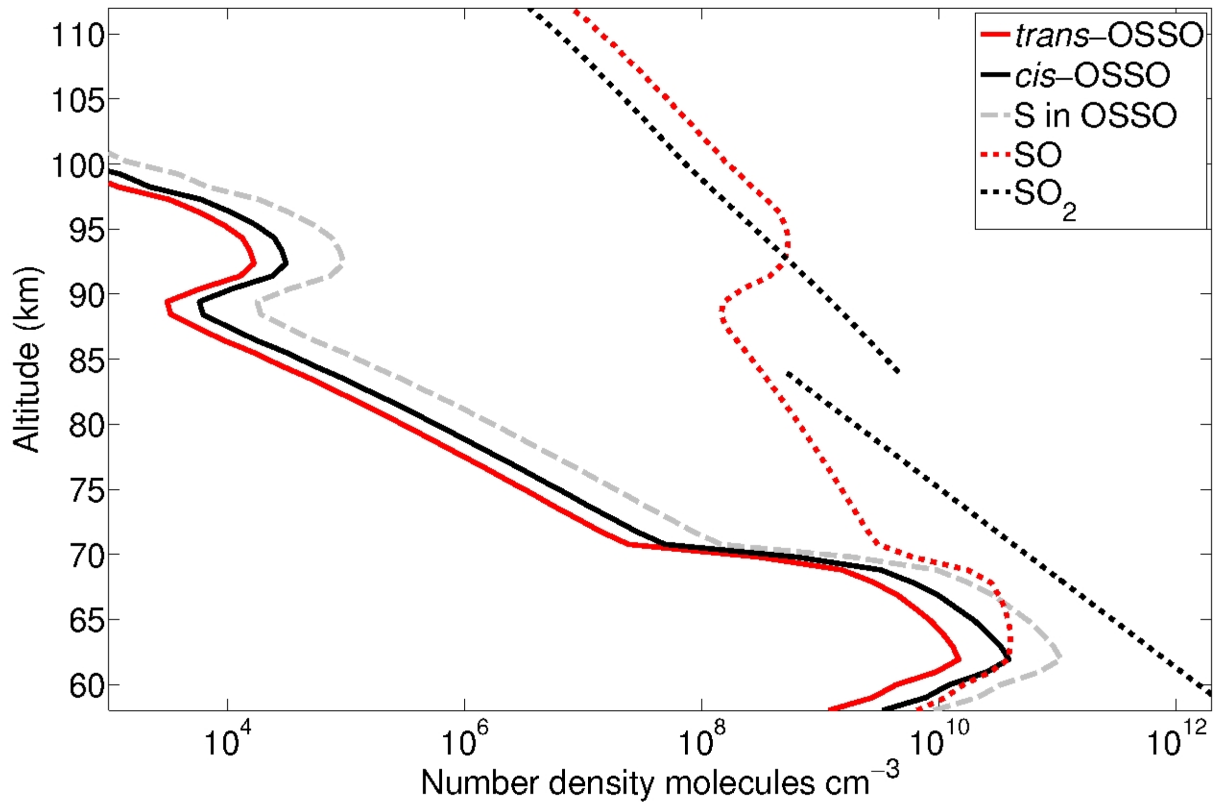

Figure S9: The altitude dependent SO_2, SO and *cis*- and *trans*-OSSO number densities in our Model A. SO number densities directly derived from Figure S8. OSSO number densities are the result of our simple 1-D model described in sections S4 and S6. The two SO_2 lines are only included for illustrative purposes and originate from the studies by Na *et al.*[22] (58-85 km altitude) and Sandor *et al.*[23] (85-112 km altitude).

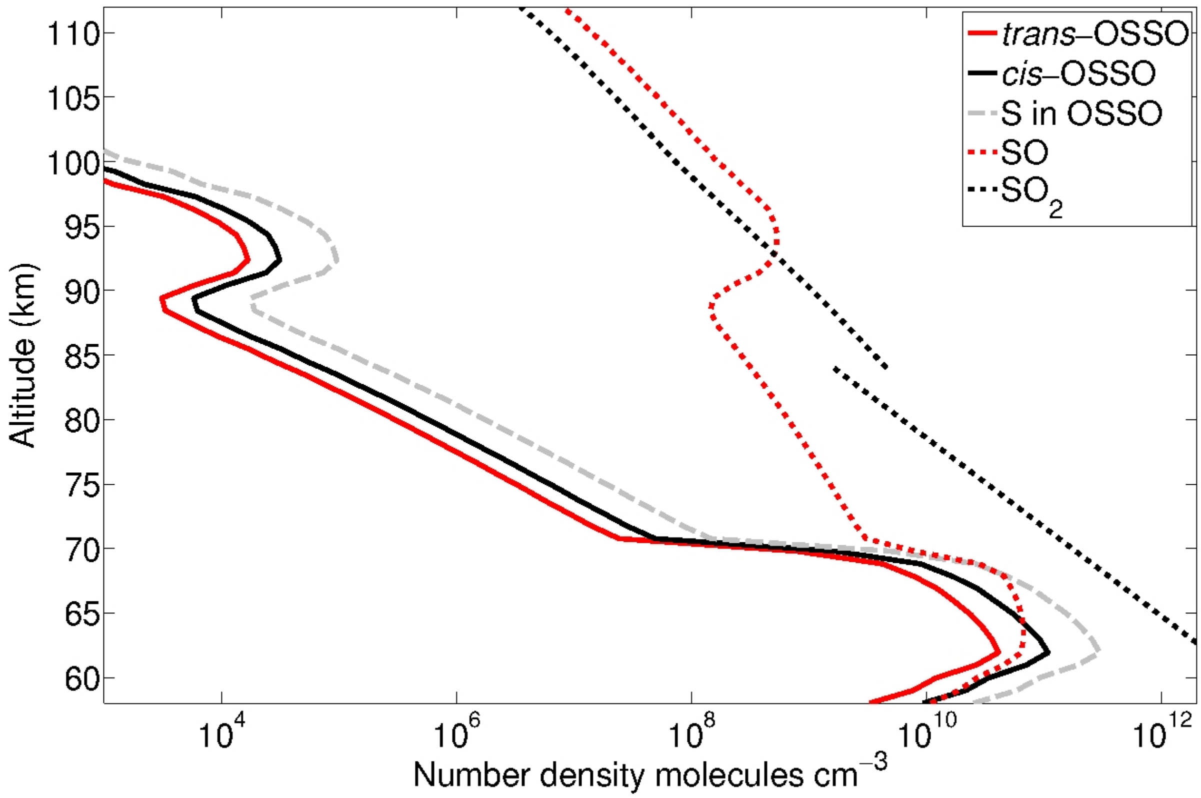

Figure S10: The altitude dependent SO_2, SO and *cis*- and *trans*-OSSO number densities in our Model B. SO number densities directly derived from Figure S8. OSSO number densities are the result of our simple 1-D model described in sections S4 and S6. The two SO_2 lines are only included for illustrative purposes and originate from the studies by Na *et al*.[25] (58-85 km altitude) and Sandor *et al*.[23] (85-112 km altitude).

References

(1) Becke, A. D. Density-functional thermochemistry. III. The role of exact exchange. *Journal Chemical Physical* **1993**, *98*, 5648–5652.

(2) Lee, C.; Yang, W.; Parr, R. G. Development of the Colle-Salvetti correlation-energy formula into a functional of the electron density. *Physical Review B* **1988**, *37*, 785–789.

(3) Zhao, Y.; Truhlar, D. G. The M06 suite of density functionals for main group thermochemistry, thermochemical kinetics, noncovalent interactions, excited states, and transition elements: two new functionals and systematic testing of four M06-class functionals and 12 other functionals. *Theoretical Chemistry Accounts* **2008**, *120*, 215–241.

(4) Chai, J.-D.; Head-Gordon, M. Long-range corrected hybrid density functionals with damped atom-atom dispersion corrections, journal=Physical Chemistry Chemical Physics **2008**, *10*, 6615–6620.

(5) Dunning T. H. Jr,; Peterson, K. A.; Wilson, A. K. Gaussian basis sets for use in correlated molecular calculations. X. The atoms aluminum through argon revisited. *Journal of Chemical Physics* **2001**, *114*, 9244–9253.

(6) Miliordos, E.; Xantheas, S. S. On the Bonding Nature of Ozone (O_3) and Its Sulfur-Substituted Analogues SO_2, OS_2, and S_3: Correlation between Their Biradical Character and Molecular Properties. *International Journal of Chemical Kinetics* **2014**, *136*, 2808–2817.

(7) Lee, T. J.; Taylor, P. R. A Diagnostic for Determining the Quality of Single-Reference Electron Correlation Methods. *International Journal of Quantum Chemistry* **1989**, *23*, 199–207.

(8) Lovas, F. J.; Tiemann, E.; Johnson, D. R. Spectroscopic studies of the SO_2 discharge system. II. Microwave spectrum of the SO dimer. *Journal of Chemical Physics* **1974**, *60*, 5005–5010.

(9) Lane, J. R.; Kjaergaard, H. G. Calculated Electronic Transitions in Sulfuric Acid and Impli-

cations for Its Photodissociation in the Atmosphere. *Journal of Physical Chemistry A* **2008**, *112*, 4958–4964.

(10) Na, C. Y.; Esposito, L. W. Is Disulfur Monoxide a Second Absorber on Venus? *Icarus* **1997**, *125*, 364–368.

(11) Krasnopolsky, V. A. Chemical composition of Venus atmosphere and clouds: Some unsolved problems. *Planetary Space and Science* **2006**, *54*, 13–14.

(12) Vandaele, A. C.; Hermans, C.; Simon, P. C.; Roozendael, M. V. Fourier Transform Measurement of NO_2 Absorption Cross-Section in the Visible Range at Room Temperature. *Journal of atmospheric Chemistry* **1996**, *25*, 289–305.

(13) Zhang, X.; Liang, M.-C.; Mills, F. P.; Belyaev, D. A.; Yung, Y. L. Sulfur chemistry in the middle atmosphere of Venus. *Icarus* **2012**, *217*, 714–739.

(14) Buchachenko, A. L. Recent advances in spin chemistry*. *Pure Applied Chemistry* **2000**, *72*, 2243–2258.

(15) Goodarzi, M.; Vahedpour, M.; Nazari, F. Theoretical study on the atmospheric formation of cis and trans-OSSO complexes. *Chemical Physics Letters* **2010**, *494*, 315–322.

(16) Murakami, Y.; Onishi, S.; Kobayashi, T.; Fujii, N.; Isshiki, N.; Tsuchiya, K.; Tezaki, A.; Matsui, K. High Temperature Reaction of $S+SO_2$->SO+SO: Implication of S_2O_2 Intermediate Complex Formation. *Journal of Physical Chemistry* **2003**, *107*, 10996–11000.

(17) Troe, J. Predictive Possibilities of Unimolecular Rate Theory. *The Journal of Physical Chemistry* **1979**, *83*, 114–126.

(18) Krasnopolsky, V. A. A photochemical model for the Venus atmosphere at 47-112 km. *Icarus* **2012**, *218*, 230–246.

(19) Herron, J. T.; Huie, R. E. Rate Constants at 298 K for the Reactions $SO+SO+M \Rightarrow (SO)_2+M$ and $SO+(SO)_2 \Rightarrow SO_2+S_2O$. *Chemical Physics Letters* **1980**, *76*, 322–324.

(20) Kánnar, D.; Szalay, P. Benchmarking Coupled Cluster Methods on Valence Singlet Excited States. *Journal of Chemical Theory and Computation* **2014**, *10*, 3757–3765.

(21) Seiff, A.; Schofield, J. T.; Kliore, A. J.; Taylor, F. W.; Limaye, S. S.; Revercomb, H. E.; Sromovsky, L. A.; Kerzhanovich, V. V.; Moroz, V. I.; Marov, M. Y. Models of the structure of the atmosphere of Venus from the surface to 100 kilometers altitude. *Advances in Space Research* **1985**, *5*, 3–58.

(22) Na, C. Y.; Esposito, L. W.; McClintock, W. E.; Barth, C. A. Sulfur Dioxide in the Atmosphere of Venus II. Modeling Results. *Icarus* **1994**, *112*, 389–395.

(23) Sandor, B. J.; Clancy, R. T.; Moriarty-Schieven, G.; Mills, F. P. Sulfur chemistry in the Venus mesosphere from SO_2 and SO microwave spectra. *Icarus* **2010**, *208*, 740–751.

(24) Belyaev, D. A.; Montmessin, F.; Bertaux, J. L.; Mahieux, A.; Fedorova, A. A.; Korablev, O. I.; Marcq, E.; Yung, Y. L.; Zhang, X. Vertical profiling of SO_2 and SO above Venus' clouds by SPICAV/SOIR solar occulations. *Icarus* **2012**, *217*, 740–751.

(25) Na, C. Y.; Esposito, L. W.; Skinner, T. E. International Ultraviolet Explorer Observation of Venus SO_2 and SO. *Journal of Geophysical Research* **1990**, *95*, 7485–7491.

(26) Rossow, W. B.; Del Genio, A. D.; Eichler, T. Cloud-Tracked Winds from *Pioneer Venus* OCPP Images. *Journal of the Atmospheric Sciences* **1990**, *47*, 2053–2084.